

# Spatial multiplexing of soliton microcombs

E. Lucas,<sup>1</sup> G. Lihachev,<sup>2,3</sup> R. Bouchand,<sup>1</sup> N. G. Pavlov,<sup>3,4</sup> A. S. Raja,<sup>1</sup> M. Karpov,<sup>1</sup> M. L. Gorodetsky,<sup>2,3</sup> and T. J. Kippenberg<sup>1,\*</sup>

<sup>1</sup>*IPHYS, École Polytechnique Fédérale de Lausanne (EPFL), CH-1015 Lausanne, Switzerland*

<sup>2</sup>*Faculty of Physics, M.V. Lomonosov Moscow State University, 119991 Moscow, Russia*

<sup>3</sup>*Russian Quantum Centre, 143025, Skolkovo, Russia*

<sup>4</sup>*Moscow Institute of Physics and Technology, 141700, Dolgoprudny, Russia*

Comb-based Fourier-transform spectroscopy utilizes two optical frequency combs to map the optical field's spectrum to a radio-frequency, allowing improved speed, and accuracy. Despite its promises, this scheme is compounded by the associated cost, complexity, and demanding stability requirements of multiple laser frequency combs. Here, we overcome these challenges and demonstrate simultaneous generation of multiple frequency combs from a single optical microresonator. Similar to space division multiplexing in fibre optical communication, we generate several dissipative Kerr soliton states, i.e. continuously circulating solitonic pulses driven by a continuous wave laser, in different spatial modes of a MgF<sub>2</sub> microresonator. Up to three different soliton states are produced simultaneously using a single pump laser, which enables both dual and triple frequency comb to be generated from one device. The resulting combs have excellent mutual coherence and can have substantial repetition rate differences, enabling fast acquisition speed, and effective suppression of intermodulation products. Dual-comb spectroscopy with amplitude and phase retrieval is realised with the free-running system, as well as coherent optical sampling to image the soliton dynamical instabilities. The demonstrated triple-comb source, is amenable to photonic integrated resonators and has the potential to extend comb-based spectroscopy to higher dimensionality, or enable advanced comb-based distance measurement schemes that have remained impractical with current technology.

Shortly after the inception of the optical frequency comb<sup>1</sup>, it was realised that combining two combs with slightly different repetition rates on a photodetector produces an RF interferogram that samples the optical response<sup>2,3</sup>, without scanning parts. Such dual-comb techniques have been demonstrated in both real-time<sup>4,5</sup> and mid-infrared<sup>6,7</sup> spectroscopy, distance measurements<sup>8</sup>, two way time transfer<sup>9</sup>, coherent anti-Stokes Raman spectro-imaging<sup>10</sup>, as well as photonic analogue to digital conversion<sup>11</sup>. However, facing the complexity and cost associated with operating two laser frequency combs, novel methods are actively explored with a view to reduce the system complexity and inherently improve the mutual coherence. For example, instead of phase locking

two independent conventional mode-locked lasers, both combs can be generated in the same laser cavity<sup>12</sup> or spectrally broadened in the same fibre in opposite propagation directions<sup>13</sup>. As the noise sources are common mode, the relative coherence between the combs is significantly improved, allowing for longer coherent averaging<sup>3</sup>.

In spatial division multiplexing, different spatial modes of an optical fibre are used as additional parallel channels to transmit data. Due to the constant rise of data traffic, this technique is becoming progressively more relevant<sup>14</sup> for increasing the capacity of optical fibres, as demonstrated by using few-mode fibres<sup>15</sup>. Similar to optical fibres, optical microresonators in general also exhibit multiple spatial mode families, that can provide additional degrees of freedom in which light can propagate, providing for example, a way to phase match second harmonic generation<sup>16</sup>. Here we demonstrate spatial multiplexing of dissipative Kerr solitons<sup>17</sup> (DKS) in a microresonator, i.e. the simultaneous generation of DKS states in several spatial modes of a resonator. DKSs are self-localised pulses of light circulating in coherently-driven passive optical resonators with Kerr nonlinearity<sup>18,19</sup>, and have been observed to spontaneously form in the context of Kerr frequency comb generation<sup>20</sup>. The coherent and broadband properties of DKS-based 'micro-combs' have already found applications in self-referencing<sup>21,22</sup>, dual-comb spectroscopy<sup>23</sup>, parallel coherent communication<sup>24</sup>, distance measurement<sup>25,26</sup>, astrophysical spectrometer calibration<sup>27,28</sup>, and photonic integrated frequency synthesis<sup>29</sup>. DKSs display rich nonlinear dynamics, covering soliton switching<sup>30</sup>, Raman self-shifting<sup>31,32</sup>, dispersive wave emission (i.e. soliton Cherenkov radiation)<sup>33</sup>, breathing solitons<sup>34</sup>, and crystallisation<sup>35</sup>. In that context, higher order spatial modes were shown to impact DKSs, causing alterations of the comb envelope via avoided mode crossing<sup>36</sup>, Cherenkov radiation emission<sup>37,38</sup>, repetition rate instability<sup>39,40</sup>, intermode breathing<sup>41</sup>, and Stokes soliton generation<sup>42</sup>. Although pumping of two orthogonally polarised modes was investigated in preliminary works<sup>43-45</sup>, it remained unexplored if independent soliton states can be generated in distinct spatial modes.

We simultaneously generate multiple soliton combs within a *single* optical microresonator by pumping up to *three* different *spatial* mode families of the same polarisation using a laser and modulation sidebands (Fig. 1c). This spatial multiplexing thereby allows not only dual but also *triple* frequency comb generation from *one and*

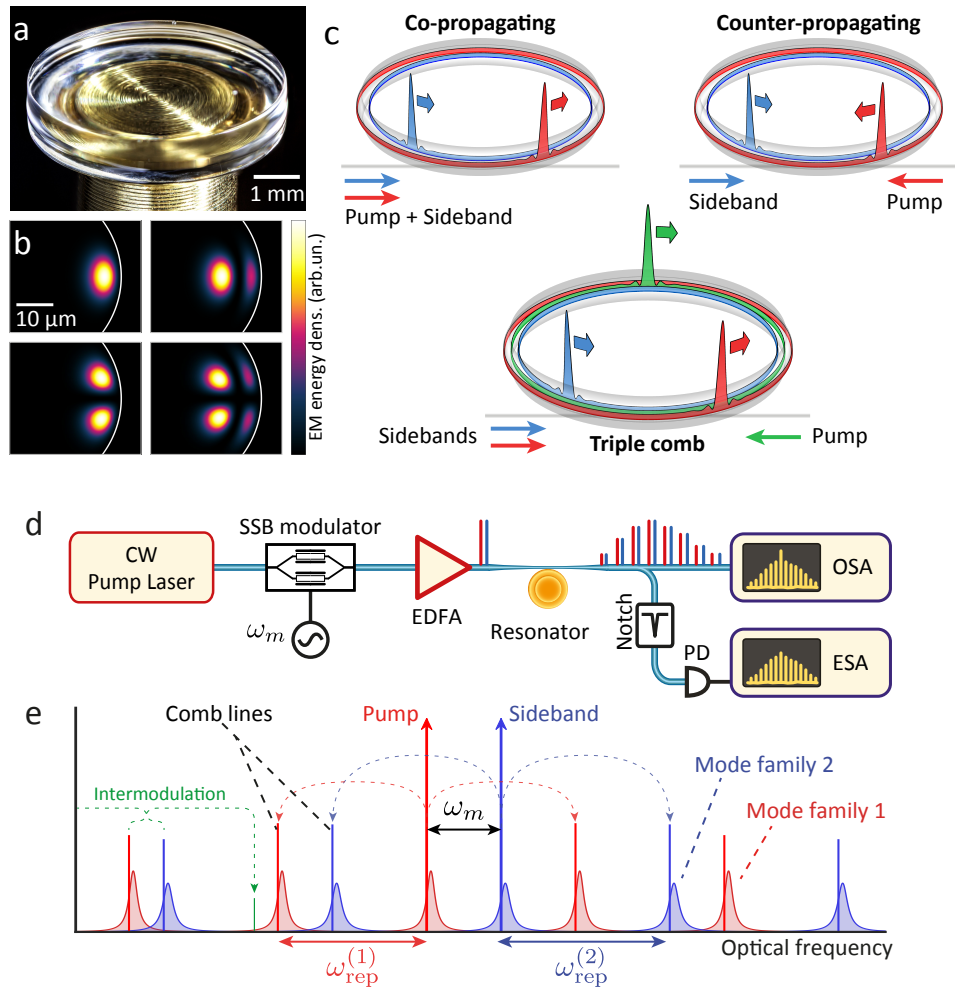


Figure 1. **Principle of spatial multiplexing of solitons in a single microresonator** (a) Crystalline  $\text{MgF}_2$  whispering gallery mode (WGM) resonator used in this work. (b) Simulation of several optical mode profiles supported by the WGM protrusion. (c) Schematic representation of the three schemes applied. (d) Setup for dual DKS generation via spatial multiplexing in the co-propagating direction. The single-sideband (SSB) modulator creates an additional carrier to pump a second mode family. EDFA: erbium doped fibre amplifier. E/O-SA: electronic/optical spectrum analyser. (e) Principle of multiplexed combs generation. The main pump laser (red arrow) is modulated to generate one sideband (blue arrow). The laser and sideband pump one resonance of two different mode families (1 in red and 2 in blue) and generate a soliton comb in each of them through the Kerr effect (red and blue lines). Co-propagating pulses may experience intermodulation effects (see SI for details).

the same device, which to the best of the authors knowledge, has not been achieved with any other laser frequency comb platform to date (e.g. Ti:Sa, semiconductor or fibre-based mode locked lasers). The distinct free spectral ranges of the respective mode families enable the generation of independent soliton pulse streams with substantial repetition rate differences (100 kHz – 100 MHz). Beyond established dual-comb techniques<sup>2,3</sup>, triple frequency comb could be utilised for higher dimensional spectroscopy, with the potential to increase information content, accuracy or speed of acquisition. Such triple laser comb source could simplify 2D coherent spectroscopy<sup>46,47</sup>, as well as advanced comb-based distance measurement schemes with increased ambiguity range<sup>48</sup>.

In the field of microcombs, for the initial demon-

strations of dual-comb applications, pairs of physically distinct yet almost identical resonators were employed<sup>23–25,49</sup>. Recent works<sup>26,50,51</sup> demonstrated the generation of dual-DKS combs with counter-propagating solitons within the same spatial mode of a *single* microresonator, using the clockwise and counter-clockwise mode degeneracy, and showed a drastic improvement of the coherence. However, this technique is limited to counter-propagating pumps and as such requires nonreciprocal elements, i.e. circulators. Moreover, since the same mode family is used, only small relative combs offset can be achieved, while the repetition rate difference is induced via the Kerr and Raman effects<sup>32</sup> and is typically moderate. As a result, the corresponding RF comb is not centred at sufficiently high frequencies, causing lines near

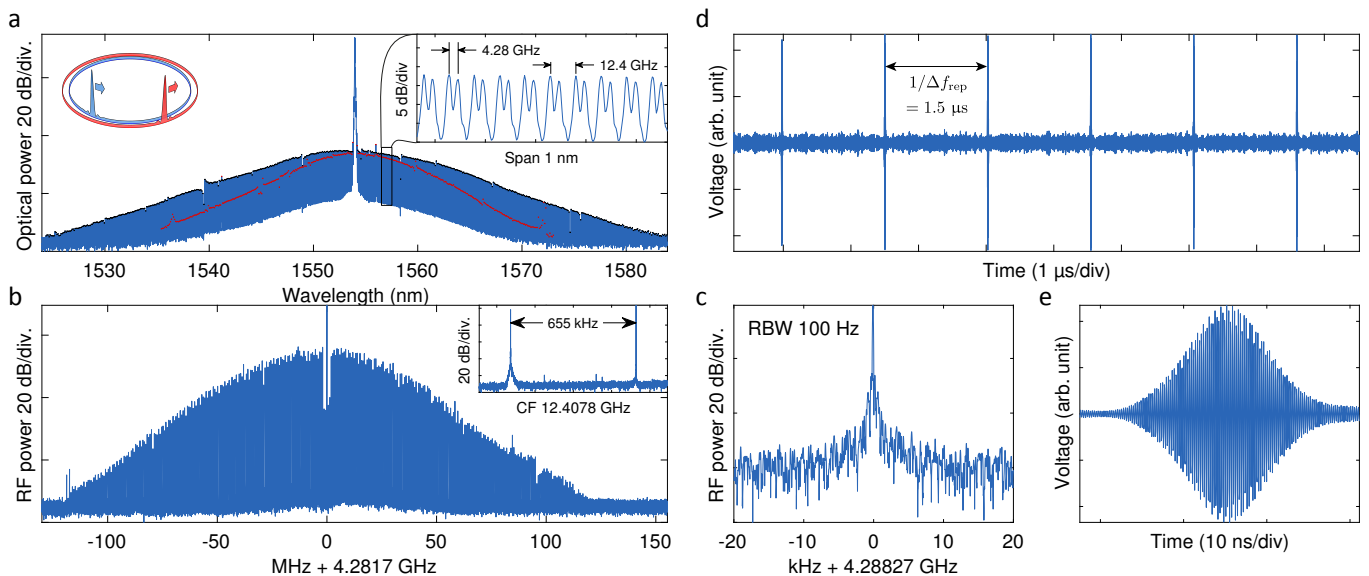


Figure 2. **Dual-comb generation with spatially-multiplexed co-propagating solitons** (a) Generated dual-comb optical spectrum. The DKS-based combs are interleaved and spaced by  $\sim 4$  GHz (see inset). The red markers delineate one comb from the other. (b) Resulting dual-comb RF heterodyne beatnotes. Resolution bandwidth (RBW): 3 kHz. The line spacing (repetition rate difference shown in inset) is 655 kHz. (c) High resolution focus of one line of the RF comb in (b). (d) Temporal interferogram of the dual-comb heterodyne shown in (b), recorded on a fast sampling oscilloscope, and after digital bandpass filtering to select the RF comb. (e) Detail of the temporal trace (d) when the two pulse overlap ( $\sim 200\times$  magnification).

DC to overlap in frequency (a consequence of mapping a portion of the lines to ‘negative’ RF frequencies), which implies that several pairs of lines beat at identical RF frequencies<sup>51</sup>. Likewise, the small repetition rate difference restricts the acquisition speed. Finally, the scheme is inherently limited by the twofold degeneracy of whispering gallery modes (WGM), only allowing dual-comb generation. The spatial multiplexing technique introduced here can overcome these shortcomings. Large repetition rate differences can be obtained, allowing shorter acquisition time. As a single laser and resonator are used, the resulting combs have thus excellent mutual coherence, and support dual-comb spectroscopy (with amplitude and phase retrieval) in spite of using a free running system. The larger offset between combs prevents soliton locking<sup>51</sup> and associated mapping ambiguity. The multiplexing can also be performed in co- or counter-propagating directions. Finally, the scalability is demonstrated with the generation of three combs in a single resonator.

We take advantage of the multi-mode nature of a crystalline  $\text{MgF}_2$  WGM cavity (Fig. 1a). Few or single mode cavity protrusions have been demonstrated<sup>52</sup> using advanced micro-machining techniques. However, the fabrication of  $\text{MgF}_2$  crystalline cavities by diamond turning and subsequent polishing with diamond slurries leads typically to multimode resonators with several mode families reaching ultrahigh quality factors ( $Q$ ) exceeding  $10^9$ . In the present work, the resonator used has a free spectral range (FSR) of 12.4 GHz, and features up to 5 mode families with the same polarisation that sustain DKS formation ( $Q \geq 10^9$ ), as shown in Fig. S.1 of the supplement-

tary information (SI).

**Spatial multiplexing with co-propagating pump fields.** We first study the use of co-propagating pumps. In this scheme (Fig. 1d,e), simultaneous pumping of two soliton-supporting resonances is achieved via electro-optical modulation. The light of an initial pump laser (external cavity diode laser, wavelength 1554 nm) passes through an IQ-modulator to generate a single sideband<sup>53</sup>, without fully suppressing the carrier, such that both reach the same power level. This creates two mutually phase-coherent carriers with a tunable frequency offset. The modulation frequency is set to  $f_m = \omega_m/2\pi \sim 4.28$  GHz to match the separation of two soliton-supporting resonances, which belong to different spatial mode families but have the same polarisation. The ‘laser scanning technique’<sup>17</sup> is subsequently applied on the main pump laser to trigger DKS formation in both mode families simultaneously. A successful tuning is however challenging as each resonance induces a thermal shift. This is mitigated in two ways: the laser is tuned across the resonances using the diode current, which allows tuning speeds faster than the thermal relaxation time of the cavity (typically ms timescale). Second, the modulation frequency  $f_m$  is carefully adjusted so that the ‘high detuning end’ of the soliton step<sup>39</sup> approximately coincide (Fig. S.1b-c). We observed that this maximises the chance of a successful tuning, and allows for simultaneous dual DKS initiation. After generation, the main laser is locked to the microresonator via offset Pound-Drever-Hall locking<sup>40</sup> and the dual-DKS combs can be stably maintained for more than 12 hours.

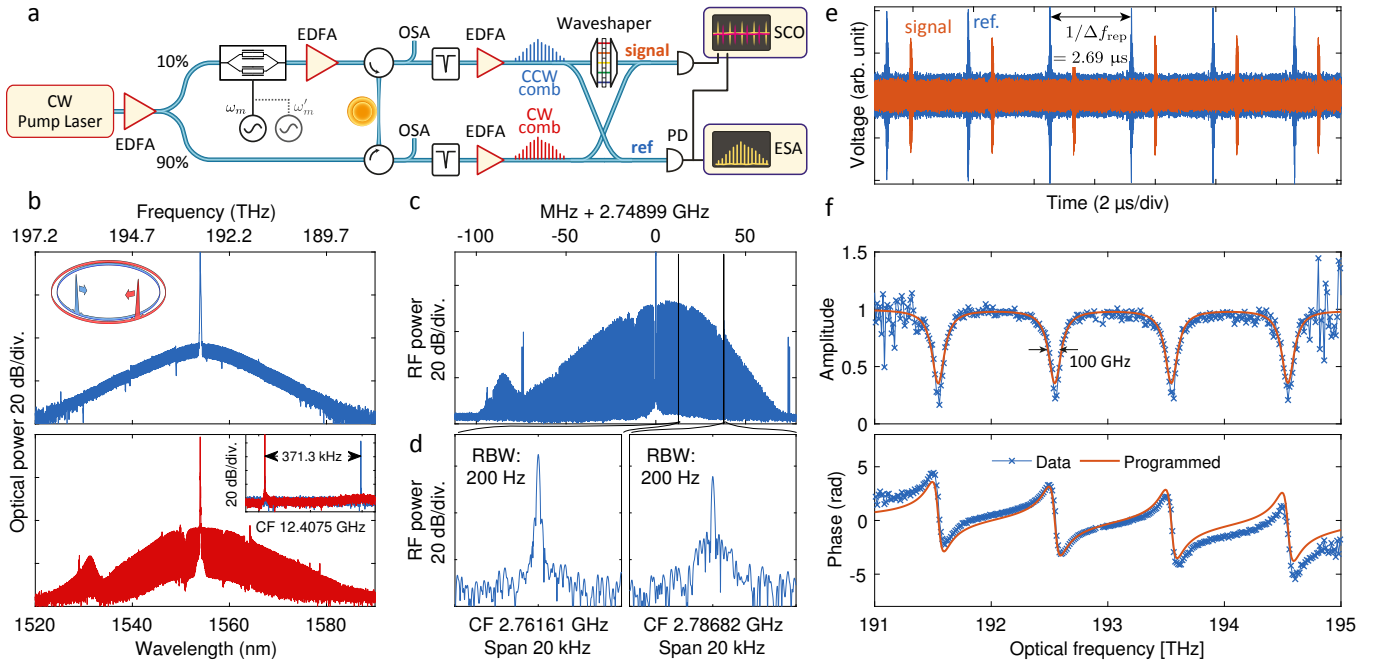


**Figure 3. Dual-comb generation with spatially multiplexed counter-propagating solitons and proof-of-principle spectroscopy** (a) Setup for counter-propagating dual and triple DKS-comb generation and spectroscopy. (b) Optical spectra of the two counter-propagating combs. (c) Resulting dual-comb beatnote (RBW 3 kHz). (d) High resolution spectra of two lines of the RF comb in (c). (e) Temporal interferogram of the dual-comb heterodyne for the signal path (with wave shaper) and reference path. (f) Retrieved amplitude and phase of the signal interferogram produced by coupling the dual-soliton pulse trains through a wave shaper programmed with synthetic absorption features (100 GHz FWHM). The orange lines display the programmed functions.

In this manner two simultaneous streams of DKSs are produced. The optical spectrum of the microresonator output (Fig. 2a) shows the two interleaved DKS combs offset by  $f_m$ . The repetition rates of the two combs differ by  $\Delta f_{\text{rep}} = 655$  kHz (around 12.4 GHz). This corresponds to a relatively small spectral compression factor<sup>3</sup> of  $m = f_{\text{rep}}/\Delta f_{\text{rep}} = 1.8 \times 10^4$ , which is useful to increase the acquisition speed of a moderate optical span. The beating of the dual-comb results here in an RF comb centred at  $f_m = 4.28$  GHz. The individual lines of the RF comb are still *resolution-limited* at 100 Hz bandwidth, although the system is free running. Owing to the high offset frequency  $f_m$ , no signs of inter-soliton locking<sup>51</sup> were observed and the total  $\sim 200$  MHz span of the RF comb maps into the corresponding 3 THz of optical span. It is important to note, that although the solitons circulate in distinct spatial modes, they can interact via four-wave mixing (FWM) when co-propagating and effectively become modulated at the rate at which the solitons cross  $\Delta f_{\text{rep}}$ , as detailed in the supplementary information (SI, cf. Fig. S.3). The modulation products that arise around the comb lines will beat with adjacent comb lines at frequencies identical to the RF comb and may thus induce optical-to-RF mapping ambiguities. In the present case, the relative strength of the first intermodulation sideband is approximately  $-20$  dBc (see Fig. S.3e), in agreement with the effect of cavity filtering.

Another pair of mode families can be selected to achieve a larger repetition rate difference if a faster acquisition is targeted (see Fig. S.2,  $\Delta f_{\text{rep}} = 9.3$  MHz, compression  $m = 1.4 \times 10^3$ ). Increasing  $\Delta f_{\text{rep}}$  enables even stronger intermodulation suppression ( $\sim -40$  dBc here) as the sidebands are created well outside the cavity bandwidth (see SI, Fig. S.3f). These experiments illustrate flexibility of the technique and its potential to substantially increase the bandwidth of the dual-comb interferogram and acquisition speed, compared with prior schemes using counter-propagating solitons<sup>51</sup>. Although a collinear dual-comb is not always suitable, co-propagating soliton generation simplifies the scheme considerably, as it lifts the need for nonreciprocal devices. Furthermore, two combs generated this way could be separated via de-multiplexing, if the offset  $f_m$  is high enough (e.g. beyond 25 GHz), which should be possible for integrated micro-resonators with larger FSR ( $> 100$  GHz).

**Spatial multiplexing in the counter-propagating configuration.** Alternatively, the two spatial mode families can be excited in a counter-propagating way, analogous to previous implementations<sup>50,51</sup>. First, the pump laser is split unevenly between two paths. A pair of circulators is then used to couple light into the resonator and to collect the transmitted combs on both sides (Fig. 3). 90% of the pump power is coupled directly into the counter-clockwise (CCW) direction. In the other path,

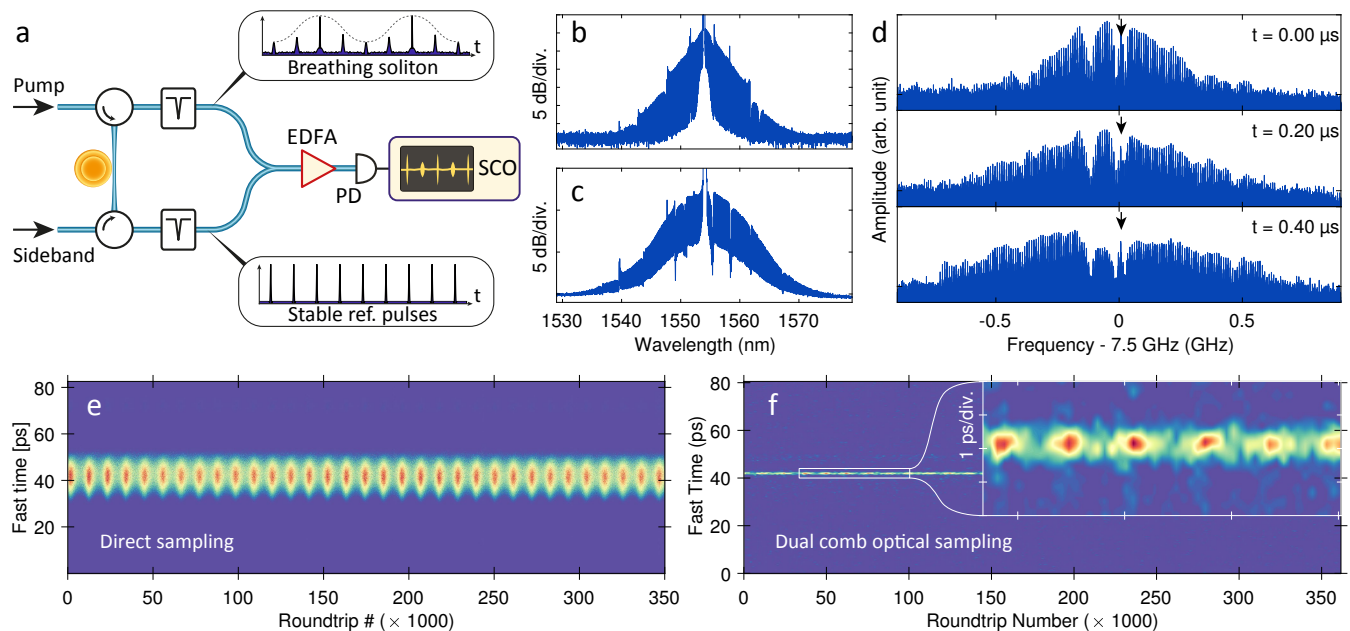


Figure 4. **Resolving the breathing dynamics of a soliton** (a) Experimental setup for breathing DKS dual comb imaging. (b) Optical spectrum of the breathing soliton pulse train and (c) of the stable reference pulse train. (d) RF spectrogram of the breathing soliton interferogram taken at maximum spectral contraction ( $t = 0 \mu s$ ) and expansion ( $t = 0.4 \mu s$ ). The arrow marks the pump position. (e) Spatiotemporal imaging of a breathing DKS via direct real-time sampling of the pulse train. (f) Same measurement realised with the multiplexed dual-comb.

the remaining 10% of the pump is sent through a single sideband modulator operated in carrier-suppressing mode to frequency-shift the light by the offset separating the two resonances. After amplification, the frequency-shifted light is coupled in the clockwise (CW) direction.

We used another set of mode families whose resonance offset is  $f_m = 2.75$  GHz, and the repetition rate difference is  $\Delta f_{\text{rep}} = 371$  kHz to demonstrate the counter-clockwise spatial multiplexing of DKSs. The soliton formation is triggered in the same way as in the co-propagating case. The two generated single-soliton combs are shown in Fig. 3, and the corresponding RF comb (Fig. 3) features a similar degree of stability to the co-propagating scheme, with 200 Hz wide beatnotes throughout the RF comb (Fig. 3d). In the counter-propagating case, no intermodulation sidebands were observed (Fig. S.3g). This is to be expected, as in this case, the FWM process between two different combs is momentum-forbidden (see SI for details).

The main advantage of the counter-propagating pump configuration is that the combs can be accessed individually, which makes the method compatible with a wide range of dual-comb applications. As a proof of concept spectroscopy experiment, one comb is sent through a waveshaper before interfering with the second comb. The beating is recorded on a high sampling rate oscilloscope (1 ms acquisition time, corresponding to  $\sim 370$  averages). The amplitude and phase of the RF comb teeth are compared to a reference signal recorded without the waveshaper. Figure 3 shows that the retrieved amplitude and

phase closely match the programmed synthetic resonance profiles over a span of 4 THz.

Rapid coherent linear optical sampling<sup>54,55</sup> was also realised to resolve the dynamics of a DKS pulse breathing at  $\sim 1$  MHz<sup>34,56</sup>. The fast recording of the dual DKS-comb multi-heterodyne offers indeed the possibility to spectrally resolve the soliton dynamics in the microresonator. To this end, another pair of mode families yielding a higher repetition rate difference ( $\Delta f_{\text{rep}} = 9.3$  MHz) is selected. The multiplexing scheme in counter-propagation is applied and the detuning in each direction is carefully set in order to generate a CCW breathing pulse and a stable DKS in CW direction (Fig. 4a). The optical spectra of each pulse trains can be viewed in panels b and c. The breathing soliton spectrum features a typical triangular profile on the optical spectrum analyser due to the averaging of the periodic spectral broadening and compression. The real-time spectral evolution of the breathing soliton can be retrieved by taking the Fourier transform to the dual comb interferogram (Fig. 4d, see SI for details). The salient features of breathing DKS can be retrieved<sup>56</sup>: over half a breathing period, the spectrum contracts and expands. Furthermore, the comb lines located near the pump are oscillating out of phase from the wing. The detection of the dual comb interferogram envelope allows the spatiotemporal dynamics of the breathing soliton to be mapped. After accounting for the compression ratio of the dual comb acquisition, this method yields an effective temporal resolution of  $\sim 1$  ps (Fig. 4f) and represents a 10

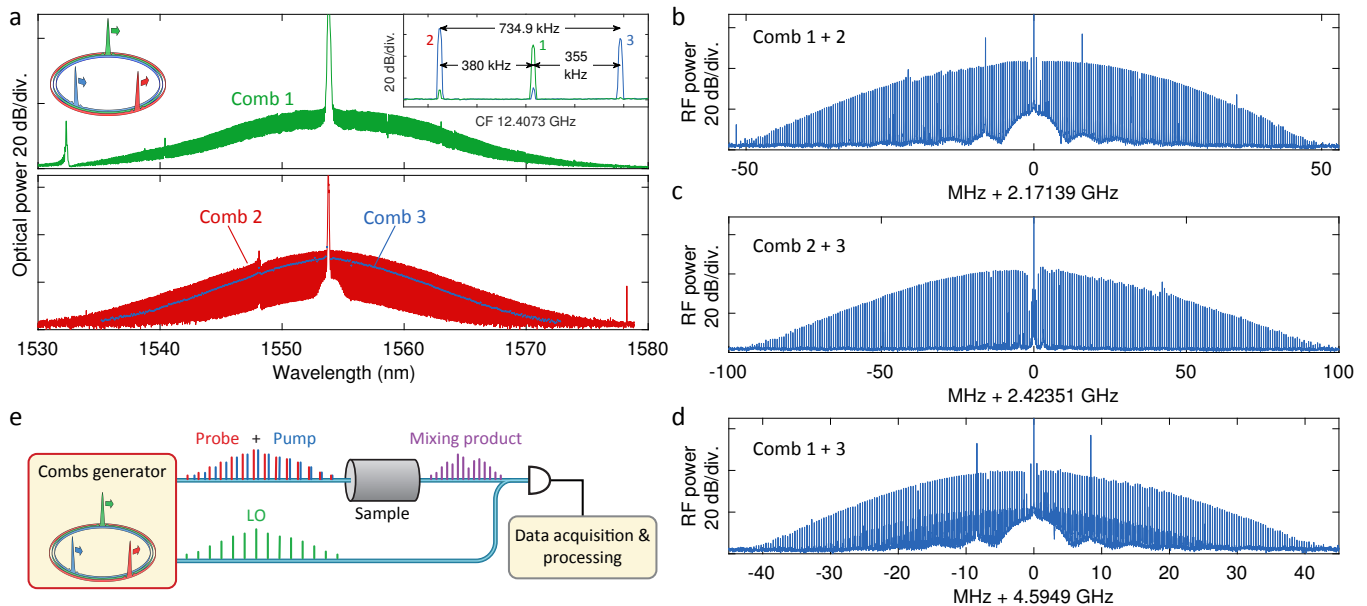


Figure 5. **Triple comb generation in a single resonator by multiplexing in three mode families** (a) Optical spectra. Comb 1 is generated in the CCW direction, while Comb 2 and 3 are generated in the CW direction. The inset shows the three distinct repetition rate beats. (b-d) Heterodyning the three pulse trains on the same photodiode leads to the formation of three RF combs (RBW 3 kHz). (e) Envisioned application of the triple comb generator for two-dimensional dual-comb spectroscopy.

fold improvement compared to the direct real-time sampling method (Fig. 4e, see SI for details).

**Triple soliton comb generation via spatial multiplexing.** We next demonstrate the ability to multiplex three soliton combs by pumping three mode families simultaneously. We employ the counter-propagating configuration, but combine two tones on the modulator (Fig. 3):  $f_m = \omega_m/2\pi = 2.17$  GHz and  $f'_m = \omega'_m/2\pi = 4.59$  GHz. This allows two mode families to be co-pumped, and thus the creation of two combs in the CW direction, while another comb is generated (Fig. 3) by pumping a third mode family in the CCW direction. Remarkably, the excitation technique outlined earlier, was also applied successfully to generate all three single soliton state combs (Fig. 5a,b). Heterodyning the combs creates a set of three RF combs centred at  $f_m$ ,  $f'_m$  and  $|f'_m - f_m| = 2.42$  GHz and with a line spacing of 380 kHz, 355 kHz, and 735 kHz respectively. In the heterodyne RF combs between the CCW and each of the CW combs, we are able to observe weak additional lines resulting from the intermodulation products on each of the CW soliton combs (Fig. 5b,d). Importantly, these additional beat-note products give rise to spectrally distinct frequencies and can thus be removed during signal processing, and critically do not induce mapping ambiguities.

The triple soliton comb configuration with two co-propagating combs could find applications in advanced spectroscopy schemes such as two-dimensional spectroscopy<sup>47</sup>, where pump and probe pulse trains are mixed in a sample and the mixing result is heterodyned with a third local oscillator comb<sup>46</sup>, as illustrated in Fig. 3e.

Optical distance measurements can also benefit from this triple comb scheme, as sending a pair of combs onto the target would provide two series of synthetic wavelength chains<sup>48</sup>, allowing a great extension of the ambiguity range<sup>8</sup> without compromising the resolution.

In summary, spatial multiplexing of soliton combs in a single microresonator is demonstrated experimentally for the first time, both in co- and counter-propagating pump configuration. The multiple soliton pulse streams have excellent mutual coherence, and their frequency offset is a substantial fraction of the repetition rate, which prevents mapping to negative frequencies. The generated dual-combs are shown to be suitable for spectroscopy. Large relative differences in repetition rates can be obtained, enabling fast acquisition and improved bandwidth usage. Using the birefringence of MgF<sub>2</sub> even larger differences are possible, when pumping modes with orthogonal polarisations (> 100 MHz were observed). When combined with faster repetition rates, such configurations could find applications in RF signal processing and acquisition<sup>57</sup>, or for ultra-rapid vibrational spectroscopy in condensed matter. The fast recording of a dual DKS-comb heterodyne can also prove useful to investigate soliton dynamics with unprecedented resolution, such as measuring the line-by-line spectral dynamics of a breathing soliton. We also demonstrate that a high repetition rate difference is also beneficial to suppress the intermodulation products when the solitons are co-propagating (as shown in Fig. S.3c).

Our work highlights the critical importance of microresonator mode engineering for comb generation,

which is already within reach of microfabricated ring resonators<sup>58,59</sup>. In the future, new designs will allow the control of the mode frequency separation and repetition rate difference, while mitigating the impact of modal crossing. Furthermore, waveguide geometric dispersion control will enable larger bandwidth coverage<sup>33,59</sup> and central wavelength selectivity<sup>60,61</sup>. The simplicity of the co-propagating scheme makes it compatible with full on-chip integration, as all the elements are readily available

in photonic integrated circuits.

The method is flexible and easily scalable, as shown by the generation of three simultaneous soliton combs – so far out of reach for other frequency comb platforms. This multiple comb source has the potential to extend frequency comb based spectroscopy to higher dimensionality, for greater information content, accuracy or speed of acquisition.

- 
- \* tobias.kippenberg@epfl.ch
- <sup>1</sup> T. W. Hansch, *Rev. Mod. Phys.* **78**, 1297 (2006).
  - <sup>2</sup> F. Keilmann, C. Gohle, and R. Holzwarth, *Optics letters* **29**, 1542 (2004).
  - <sup>3</sup> I. Coddington, N. Newbury, and W. Swann, *Optica* **3**, 414 (2016).
  - <sup>4</sup> A. Schliesser and R. Mirzoyan, *Astropart. Phys.* **24**, 382 (2005).
  - <sup>5</sup> T. Ideguchi, A. Poisson, G. Guelachvili, N. Picqué, and T. W. Hänsch, *Nature communications* **5**, 3375 (2014).
  - <sup>6</sup> A. Hugi, G. Villares, S. Blaser, H. C. Liu, and J. Faist, *Nature* **492**, 229 (2012).
  - <sup>7</sup> G. Villares, A. Hugi, S. Blaser, and J. Faist, *Nature Communications* **5**, 1 (2014).
  - <sup>8</sup> I. Coddington, W. C. Swann, L. Nenadovic, and N. R. Newbury, *Nature Photonics* **3**, 351 (2009).
  - <sup>9</sup> L. C. Sinclair, H. Bergeron, W. C. Swann, E. Baumann, J.-D. Deschênes, and N. R. Newbury, *Physical Review Letters* **120**, 1 (2017).
  - <sup>10</sup> T. Ideguchi, S. Holzner, B. Bernhardt, G. Guelachvili, N. Picqué, T. W. Hänsch, N. Picque, and T. W. Hansch, *Nature* **502**, 355 (2013).
  - <sup>11</sup> X. Yang, K. Xu, J. Yin, Y. Dai, F. Yin, J. Li, H. Lu, T. Liu, and Y. Ji, *Optics Express* **22**, 869 (2014).
  - <sup>12</sup> S. M. Link, D. J. H. C. Maas, D. Waldburger, and U. Keller, *Science* **356**, 1164 (2017).
  - <sup>13</sup> G. Millot, S. Pitois, M. Yan, T. Hovhannisyanyan, A. Bendahmane, T. W. Hänsch, and N. Picqué, *Nature Photonics* **10**, 27 (2015).
  - <sup>14</sup> D. J. Richardson, J. M. Fini, and L. E. Nelson, *Nature Photonics* **7**, 354 (2013).
  - <sup>15</sup> N. Bozinovic, Y. Yue, Y. Ren, M. Tur, P. Kristensen, H. Huang, A. E. Willner, and S. Ramachandran, *Science* **340**, 1545 (2013).
  - <sup>16</sup> X. Guo, C.-L. Zou, and H. X. Tang, *Optica* **3**, 1126 (2016).
  - <sup>17</sup> T. Herr, V. Brasch, J. D. Jost, C. Y. Wang, N. M. Kondratiev, M. L. Gorodetsky, and T. J. Kippenberg, *Nature Photonics* **8**, 145 (2013).
  - <sup>18</sup> F. Leo, S. Coen, P. Kockaert, S.-P. Gorza, P. Emplit, and M. Haelterman, *Nature Photonics* **4**, 471 (2010).
  - <sup>19</sup> L. A. Lugiato and R. Lefever, *Physical review letters* **58**, 2209 (1987).
  - <sup>20</sup> P. Del’Haye, A. Schliesser, O. Arcizet, T. Wilken, R. Holzwarth, and T. J. Kippenberg, *Nature* **450**, 1214 (2007).
  - <sup>21</sup> J. D. Jost, T. Herr, C. Lecaplain, V. Brasch, M. H. P. Pfeiffer, and T. J. Kippenberg, *Optica* **2**, 706 (2015).
  - <sup>22</sup> V. Brasch, E. Lucas, J. D. Jost, M. Geiselmann, and T. J. Kippenberg, *Light Sci Appl.* **6**, e16202 (2017).
  - <sup>23</sup> M. G. Suh, Q. F. Yang, K. Y. Yang, X. Yi, and K. J. Vahala, *Science* **354**, 600 (2016).
  - <sup>24</sup> P. Marin-Palomo, J. N. Kemal, M. Karpov, A. Kordts, J. Pfeifle, M. H. P. Pfeiffer, P. Trocha, S. Wolf, V. Brasch, M. H. Anderson, R. Rosenberger, K. Vijayan, W. Freude, T. J. Kippenberg, and C. Koos, *Nature* **546**, 274 (2017).
  - <sup>25</sup> P. Trocha, M. Karpov, D. Ganin, M. H. P. Pfeiffer, A. Kordts, S. Wolf, J. Krockenberger, P. Marin-Palomo, C. Weimann, S. Randel, W. Freude, T. J. Kippenberg, and C. Koos, *Science* **359**, 887 (2018).
  - <sup>26</sup> M.-G. Suh and K. J. Vahala, *Science* **359**, 884 (2018).
  - <sup>27</sup> M.-G. Suh, X. Yi, Y.-H. Lai, S. Leifer, I. S. Grudin, G. Vasisht, E. C. Martin, M. P. Fitzgerald, G. Doppmann, J. Wang, D. Mawet, S. B. Papp, S. A. Diddams, C. Beichman, and K. Vahala, (2018), arXiv:1801.05174.
  - <sup>28</sup> E. Ozbud, M. Rainer, A. Harutyunyan, M. H. Anderson, M. Geiselmann, B. Chazelas, S. Kundermann, S. Lecomte, M. Cecconi, A. Ghedina, E. Molinari, F. Pepe, F. Wildi, F. Bouchy, T. J. Kippenberg, and T. Herr, (2017), arXiv:1712.09526.
  - <sup>29</sup> D. T. Spencer, T. Drake, T. C. Briles, J. Stone, L. C. Sinclair, C. Fredrick, Q. Li, D. Westly, B. R. Ilic, A. Bluestone, N. Volet, T. Komljenovic, L. Chang, S. H. Lee, D. Y. Oh, M.-G. Suh, K. Y. Yang, M. H. P. Pfeiffer, T. J. Kippenberg, E. Norberg, L. Theogarajan, K. Vahala, N. R. Newbury, K. Srinivasan, J. E. Bowers, S. A. Diddams, and S. B. Papp, *Nature* **557**, 81 (2018).
  - <sup>30</sup> H. Guo, M. Karpov, E. Lucas, A. Kordts, M. H. P. Pfeiffer, V. Brasch, G. Lihachev, V. E. Lobanov, M. L. Gorodetsky, and T. J. Kippenberg, *Nature Physics* **13**, 94 (2017).
  - <sup>31</sup> D. V. Skryabin, *Science* **301**, 1705 (2003).
  - <sup>32</sup> M. Karpov, H. Guo, A. Kordts, V. Brasch, M. H. P. Pfeiffer, M. Zervas, M. Geiselmann, and T. J. Kippenberg, *Physical Review Letters* **116**, 103902 (2016).
  - <sup>33</sup> V. Brasch, M. Geiselmann, T. Herr, G. Lihachev, M. H. P. Pfeiffer, M. L. Gorodetsky, and T. J. Kippenberg, *Science* **351**, 357 (2015).
  - <sup>34</sup> E. Lucas, M. Karpov, H. Guo, M. L. Gorodetsky, and T. J. Kippenberg, *Nature Communications* **8**, 736 (2017).
  - <sup>35</sup> D. C. Cole, E. S. Lamb, P. Del’Haye, S. A. Diddams, and S. B. Papp, *Nature Photonics* **11**, 671 (2017).
  - <sup>36</sup> T. Herr, V. Brasch, J. D. Jost, I. Mirgorodskiy, G. Lihachev, M. L. Gorodetsky, and T. J. Kippenberg, *Physical Review Letters* **113**, 123901 (2014).
  - <sup>37</sup> A. B. Matsko, W. Liang, A. A. Savchenkov, D. Elyahu, and L. Maleki, *Optics Letters* **41**, 2907 (2016).
  - <sup>38</sup> Q.-F. Yang, X. Yi, K. Y. Yang, and K. Vahala, *Optica* **3**, 1132 (2016).
  - <sup>39</sup> E. Lucas, H. Guo, J. D. Jost, M. Karpov, and T. J. Kippenberg, *Physical Review A* **95**, 43822 (2017).
  - <sup>40</sup> E. Lucas, J. D. Jost, K. Beha, R. Holzwarth, and T. Kip-

- penberg, in *2017 IEEE International Frequency Control Symposium* (IEEE, 2017) pp. 530–533.
- <sup>41</sup> H. Guo, E. Lucas, M. H. P. Pfeiffer, M. Karpov, M. Anderson, J. Liu, M. Geiselmann, J. D. Jost, and T. J. Kippenberg, *Physical Review X* **7**, 041055 (2017).
- <sup>42</sup> Q. F. Yang, X. Yi, K. Y. Yang, and K. Vahala, *Nature Physics* **13**, 53 (2017).
- <sup>43</sup> C. Bao, P. Liao, A. Kordts, L. Zhang, A. Matsko, M. Karpov, M. H. P. Pfeiffer, G. Xie, Y. Cao, Y. Yan, A. Al-maiman, Z. Zhao, A. Mohajerin-Ariaei, A. Fallahpour, F. Alishahi, M. Tur, L. Maleki, T. J. Kippenberg, and A. E. Willner, (2017), arXiv:1705.05045.
- <sup>44</sup> P. Donvalkar, F. A. Barbosa, X. Ji, Y. Okawachi, R. McNally, A. Farsi, A. Klenner, M. Lipson, A. L. Gaeta, M. Lipson, and A. L. Gaeta, in *Conference on Lasers and Electro-Optics* (OSA, Washington, D.C., 2017) p. STu4J.5.
- <sup>45</sup> X. Zhao, J. M. Silver, L. Del Bino, P. Del’Haye, L. D. Bino, and P. Del’Haye, in *Conference on Lasers and Electro-Optics* (OSA, Washington, D.C., 2017) p. STh3L.4.
- <sup>46</sup> B. Lomsadze and S. T. Cundiff, *Science* **357**, 1389 (2017).
- <sup>47</sup> S. T. Cundiff and S. Mukamel, *Physics Today* **66**, 44 (2013).
- <sup>48</sup> X. Zhao, X. Qu, F. Zhang, Y. Zhao, and G. Tang, *Optics Letters* **43**, 807 (2018).
- <sup>49</sup> A. Dutt, C. Joshi, X. Ji, J. Cardenas, Y. Okawachi, K. Luke, A. L. Gaeta, and M. Lipson, *Science Advances* **4** (2018).
- <sup>50</sup> C. Joshi, A. Klenner, Y. Okawachi, M. Yu, K. Luke, X. Ji, M. Lipson, and A. L. Gaeta, *Optics Letters* **43**, 547 (2018).
- <sup>51</sup> Q. F. Yang, X. Yi, K. Y. Yang, and K. Vahala, *Nature Photonics* **11**, 560 (2017).
- <sup>52</sup> I. S. Grudinin and N. Yu, *Optica* **2**, 221 (2015).
- <sup>53</sup> M. Izutsu, S. Shikama, and T. Sueta, *IEEE Journal of Quantum Electronics* **17**, 2225 (1981).
- <sup>54</sup> V. Durán, S. Tainta, and V. Torres-Company, *Optics Express* **23**, 30557 (2015).
- <sup>55</sup> I. Coddington, W. C. Swann, and N. R. Newbury, *Optics Letters* **34**, 2153 (2009).
- <sup>56</sup> C. Bao, J. A. Jaramillo-Villegas, Y. Xuan, D. E. Leaird, M. Qi, and A. M. Weiner, *Physical Review Letters* **117**, 163901 (2016).
- <sup>57</sup> D. Esman, V. Ataie, B. P.-P. Kuo, N. Alic, and S. Radic, *Journal of Lightwave Technology* **34**, 5214 (2016).
- <sup>58</sup> S. Kim, K. Han, C. Wang, J. A. Jaramillo-Villegas, X. Xue, C. Bao, Y. Xuan, D. E. Leaird, A. M. Weiner, and M. Qi, *Nature Communications* **8** (2017).
- <sup>59</sup> M. H. P. Pfeiffer, C. Herkommer, J. Liu, H. Guo, M. Karpov, E. Lucas, M. Zervas, and T. J. Kippenberg, *Optica* **4**, 684 (2017).
- <sup>60</sup> S. H. Lee, D. Y. Oh, Q. F. Yang, B. Shen, H. Wang, K. Y. Yang, Y. H. Lai, X. Yi, X. Li, and K. Vahala, *Nature Communications* **8**, 1 (2017).
- <sup>61</sup> M. Karpov, M. H. P. Pfeiffer, J. Liu, A. Lukashchuk, and T. J. Kippenberg, *Nature Communications* **9**, 1146 (2018).
- <sup>62</sup> X. Yi, Q.-F. Yang, K. Y. Yang, and K. Vahala, (2018), arXiv:1805.07629.

#### DATA AVAILABILITY STATEMENT

The data and code used to produce the results of this manuscript will be available on Zenodo upon publication.

#### AUTHORS CONTRIBUTIONS

E.L. and G.L. designed the experimental setup. E.L. performed the experiments and analysed the data. G.L. fabricated the device, with assistance of N.G.P.. E.L., R.B. and A.R. performed the experimental comb linewidth measurement. M.K. and A.R. assembled the RF components for the single sideband modulator driving. E.L. wrote the manuscript, with input from other authors. T.J.K. and M.L.G. supervised the project.

#### ACKNOWLEDGMENTS

The authors thank Nathan Newbury (NIST Boulder) for important suggestions and comments. The authors thank J.D. Jost and W. Weng for their assistance as well as N.J. Engelsen and M. Anderson for their feedback on the manuscript. This publication was supported by Contract W31P4Q-14-C-0050 from the Defense Advanced Research Projects Agency (DARPA), Defense Sciences Office (DSO), as well as funding from the Swiss National Science Foundation under grant agreement 163864, by the Air Force Office of Scientific Research, Air Force Material Command, USAF under Award No. FA9550-15-1-0099, and by the Ministry of Education and Science of the Russian Federation under project RFMEFI58516X0005. E.L. acknowledges the support of the European Space Technology Centre with ESA Contract No.: 4000118777/16/NL/GM.

#### SUPPLEMENTARY INFORMATION

**Resonator fabrication and characteristics** The microresonator protrusion was fabricated via ultra-precise diamond turning of a mono-crystalline  $\text{MgF}_2$  blank followed by hand polishing with diamond slurries and cleaning. The FSR of 12.4 GHz corresponds to a main radius of 2.8 mm. The resulting WGM protrusion can be approximated by an oblate spheroid with 80  $\mu\text{m}$  minor radius. The obtained quality factors of the soliton-supporting resonances are above  $10^9$  at 1554 nm.

**Soliton resonances identification** The piezo of the pump ECDL is scanned over a full FSR of the cavity at 1554 nm, while recording the transmission and the non-linearly generated light on an analogue to digital converter. Five resonances featuring the typical step transition associated with the formation of solitons<sup>17</sup> could be identified (Fig. S.1a). Their relative offset was estimated using piezo voltage calibration.

**Tuning Method** In order to initiate the dual-comb formation, we first target a pair of mode families. The pump laser is tuned close to one resonance and the modulation frequency of the sideband is set close to the resonance offset, while the bias of the SSB modulator is adjusted to generate a blue or red sideband, depending on the sign



of the frequency shift needed. After a coarse adjustment, both resonances are visible when scanning the pump laser over a small frequency span (Fig. S.1b). The final adjustment consists of tuning the sideband frequency shift so that the large detuning end of each the soliton step becomes aligned (Fig. S.1c). When scanning the laser, two solitons can then be excited simultaneously.

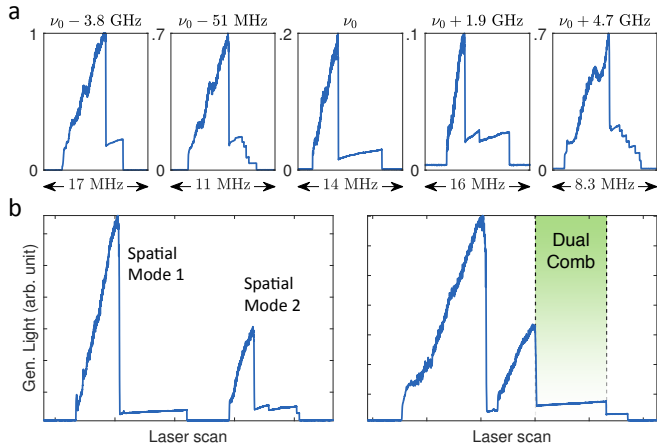


Figure S.1. (a) Identification of the soliton-supporting resonance over one cavity FSR. The graphs display the generated comb light at the output of the resonator as the laser frequency is decreased. The step features correspond to the detuning region where solitons exist. (b) Sequential excitation of two soliton-supporting resonances (in the co-propagating scheme), when the offset frequency is detuned. The left resonance is excited with the pump laser light while the right is excited with the sideband. (c) Adjusting the sideband shift allows the overlap of the resonances. The region where the two steps coexist corresponds to the formation of the dual DKS comb.

**Larger repetition rate difference via mode families selection** Several RF comb offset frequencies and repetition rate differences can be achieved in the same resonator, by changing the pair of modes supporting the solitons. In this way we could generate solitons in the co-propagating direction (Fig. S.2a) with an offset of 4.9 GHz and a repetition rate difference of  $\sim 9$  MHz. The resulting RF comb (Fig. S.2b) spans more than 4 GHz. However, this high offset frequency  $f_m$  combined with a broader comb implies that the RF comb extends beyond  $f_{\text{rep}}/2$  and thus overlaps with the mirror comb<sup>3</sup> centred at  $f_{\text{rep}} - f_m$ , leading to potential mapping ambiguities in the overlap region. Engineering the modes of the microresonator, enabled by better fabrication control, will allow an optimal bandwidth usage.

**Dual comb imaging of the soliton dynamics.** In a specific range of detuning and pump parameters, DKS can undergo a breathing instability where the solitonic pulse oscillates both in amplitude and in duration<sup>34,56</sup>. Thanks to the long photon lifetime of microresonators, the oscillation period is much longer than the roundtrip time (the breathing rate is  $\sim 1$  MHz, for a 12.7 GHz

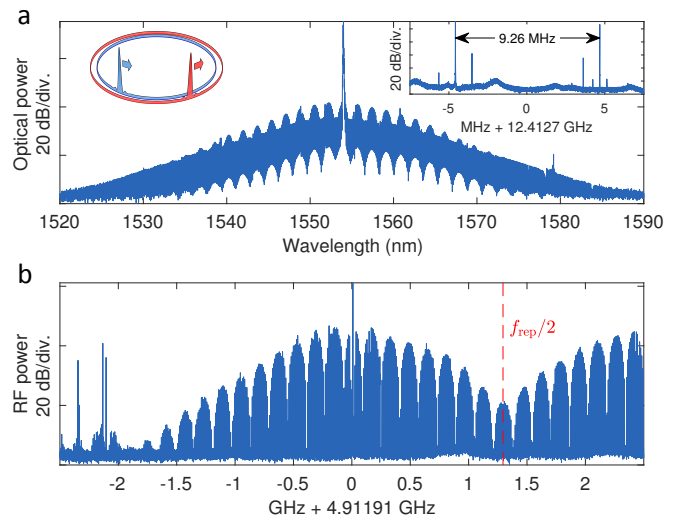


Figure S.2. (a) Generated dual-comb optical spectrum in the co-propagating direction. One of the combs corresponds to a two-soliton state and hence has a distinct spectral interference pattern. The repetition rate difference is shown in the inset. (b) Corresponding RF heterodyne comb.

repetition rate).

First, resolving the spatiotemporal dynamics of breathing solitons was carried out via direct sampling of the breathing pulse train, using a very fast photodiode ( $\sim 10$  ps impulse response) and real-time oscilloscope (120 GSa/s) in order to sample every roundtrip<sup>34</sup>. However, the fast temporal resolution of this method is limited by the photodiode impulse response and closely spaced solitons may not be distinguished (Fig. 4e), while the slow breathing evolution is oversampled and can only be monitored for a short time span at such sampling rates.

Another method is to take advantage of the dual comb principle. This method is derived from coherent linear optical sampling<sup>54,55</sup> and was applied to very recently to microcavities, using a reference electro-optic comb<sup>62</sup>. The envelope of a dual comb interferogram between a breathing soliton and a reference pulse train with a slight difference in repetition rate  $\Delta f_{\text{rep}}$  yields the convolution of the breathing pulse with the reference. The pulses overlap each  $1/\Delta f_{\text{rep}}$ , which corresponds to the time for one pulse to sweep over one entire roundtrip of the other pulse train, and sets the imaging frame rate. Thus if  $\Delta f_{\text{rep}}$  is faster than the breathing rate, the breathing dynamics can be monitored, while relaxing the requirement on the sampling rate (ultimately only to match RF comb bandwidth).

The dual comb is generated via multiplexing two solitons in counter-propagation (see Fig. 4). The mode families are selected to reach  $\Delta f_{\text{rep}} = 9.26$  MHz (one frame period is acquired over 1340 roundtrips). The real-time spectral evolution of the breathing soliton (multiplied by the reference pulse spectrum) can be retrieved by taking the Fourier transform to the dual comb interferogram

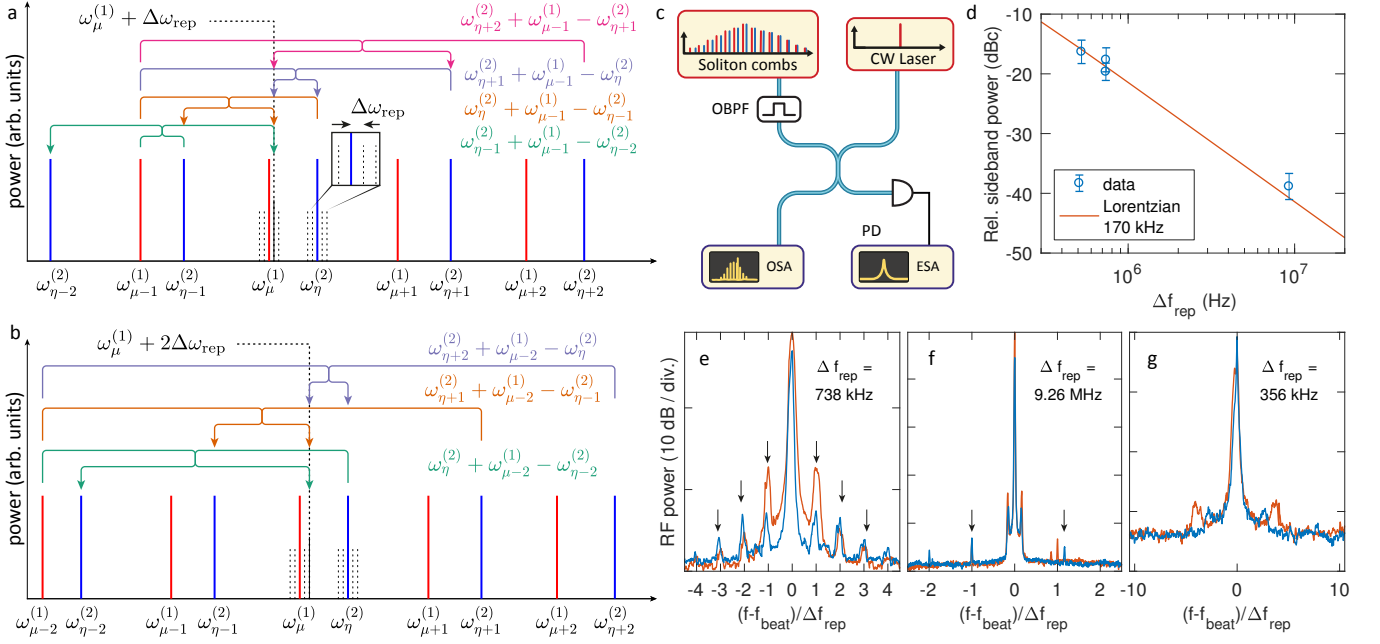


Figure S.3. **Intermodulation of co-propagating solitons** (a) Illustration of FWM processes leading to the formation of the  $+\Delta\omega_{\text{rep}}$  sideband around the comb line  $\omega_{\mu}^{(1)}$  (five comb lines are considered here, the cavity filtering is not taken into account). (b) Processes leading to the formation of the  $+2\Delta\omega_{\text{rep}}$  sideband around the comb line  $\omega_{\mu}^{(1)}$  (c) Experimental scheme used to measure the optical lineshape of the comb lines. Individual lines of each comb are heterodyned with an independent laser, after selection with an optical bandpass filter (OBPF) and the beat measured on an electronic spectrum analyser (ESA). (d) Scaling of the mean relative power in the first sidebands (at  $\pm\Delta\omega_{\text{rep}}$ ) averaged over several comb lines, for different repetition rate difference  $\Delta f_{\text{rep}} = \Delta\omega_{\text{rep}}/2\pi$ . (e) Heterodyne beatnotes of the reference laser with a line of two co-propagating combs with a repetition rate difference of  $\Delta f_{\text{rep}} = 738$  kHz (RBW 50 kHz). The black arrows show the intermodulation sidebands. (f) Same measurement in the case of  $\Delta f_{\text{rep}} = 9.26$  MHz (RBW 100 kHz). (g) Heterodyne beatnotes of the reference laser with a line of two counter-propagating combs with a repetition rate difference of  $\Delta f_{\text{rep}} = 356$  kHz (RBW 50 kHz).

(Fig. 4d). In order to improve the signal to noise ratio, multiple interferogram frames at similar breathing phases were averaged together (after multiplication by a gaussian window of width  $1/\Delta f_{\text{rep}}$ ).

To view the spatiotemporal dynamics of the breathing soliton, the interferogram envelope is retrieved via Hilbert transform and each frame is sliced and stacked (Fig. 4f). The fast time axis can be rescaled to span  $1/f_{\text{rep}}$  to account for the compression ratio of the dual comb acquisition method. Panels e and f show the vast improvement in temporal resolution of the dual comb method over the direct sampling method ( $\sim 1$  ps vs.  $\sim 10$  ps).

### Intermodulation products via inter-comb FWM for co-propagating solitons.

The two generated dissipative Kerr solitons, exhibiting different free spectral range, can in general interact and cause intermodulation products. Intermodulation of two co-propagating solitons can occur via four-wave mixing, and can lead to additional sidebands around the optical comb lines. We consider here the comb line frequencies

in the case of two combs (1) and (2):

$$\omega_{\mu}^{(1)} = \omega_p + \mu \omega_{\text{rep}}^{(1)} \quad (1)$$

$$\omega_{\eta}^{(2)} = (\omega_p + \omega_m) + \eta (\omega_{\text{rep}}^{(1)} + \Delta\omega_{\text{rep}}) \quad (2)$$

where  $(\mu, \eta)$  are the azimuthal mode numbers (relative to the pumped mode, for which  $\mu = 0$  and  $\eta = 0$ ),  $\omega_p$  the pump laser frequency,  $\omega_{\text{rep}}^{(1)}$  the repetition rate of the first comb,  $\omega_m$  the single sideband modulation frequency and  $\Delta\omega_{\text{rep}} = 2\pi\Delta f_{\text{rep}}$  the difference in repetition rate. Inter-comb four-wave mixing can occur for lines fulfilling the phase matching condition (i.e. angular momentum conservation that is  $\int d\phi \cdot e^{i(\mu+\eta-\mu'-\eta')\cdot\phi} = 1$ ):  $\mu + \eta = \mu' + \eta'$ . For counter-propagating solitons in distinct mode families, this momentum matching cannot be satisfied. However, for two co-propagating mode families for example,  $\mu + \eta = (\mu - 1) + (\eta + 1)$  is a possible path that conserves momentum, and the resulting frequencies are  $\omega_{\mu}^{(1)} + \omega_{\eta}^{(2)} = \omega_{\mu-1}^{(1)} + (\omega_{\eta+1}^{(2)} - \Delta\omega_{\text{rep}})$ . As the last frequency does not coincide with an existing comb line, and falls outside the cavity resonance, the mixing product is expected to be inefficient (and suppressed by the cavity lorentzian). Another series of FWM processes leading to the creation of the intermodulation sideband at  $\omega_{\mu}^{(1)} + \Delta\omega_{\text{rep}}$  are represented in Fig. S.3a, when consid-

ering 5 comb lines (the cavity filtering is not accounted for).

The presence of sidebands spaced by  $\Delta\omega_{\text{rep}}$  around each of the comb lines can induce optical-to-RF mapping ambiguities, as illustrated in Fig. S.4. The beat between lines  $\omega_{\mu}^{(1)}$  and  $\omega_{\mu}^{(2)}$  results in the frequency  $\omega_{\mu}^{(2)} - \omega_{\mu}^{(1)} = \omega_m + \mu \Delta\omega_{\text{rep}}$ . However, the beat between the adjacent lines  $\pm\mu$  and their sidebands as well as a pair of sidebands around  $\mu\pm 2$  will be at an identical frequency. Therefore, importantly, the presence of sidebands around the comb lines does not appear in the RF dual-comb spectrum, but can be evidenced by the appearance of several lines spaced by  $\Delta\omega_{\text{rep}}$  around the repetition rates of the combs (or by a high resolution recording of the optical spectrum). Note that in the present experiments the cross products of a comb line and a sideband are attenuated by the relative amplitude of the sidebands i.e. at least 20 dB.

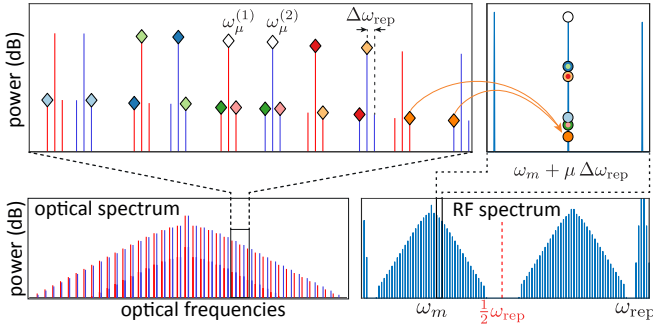


Figure S.4. Illustration of the mapping ambiguity induced by the intermodulation sidebands around the comb lines. The lines  $\omega_{\mu}^{(1)}$  and  $\omega_{\mu}^{(2)}$  beat at a frequency  $\omega_m + \mu \Delta\omega_{\text{rep}}$ , which is the same frequency as the beating between adjacent lines / sidebands. The pairs of optical lines / sidebands beating at the same frequencies are marked with identical colour (top left, the spacing of the sidebands was expanded for visualization) and their corresponding mixing in the RF domain is indicated by a dot with the matching colour (top right).

Experimentally, we evaluated the strength of the intermodulation sidebands by beating several lines of each soliton comb with another reference laser centred at 1556.5 nm (Fig. S.3c), having an optical linewidth of  $\sim 30$  kHz. If the solitons are co-propagating (Fig. S.3d-f), sidebands at  $\Delta\omega_{\text{rep}}$  can be clearly identified. This measurement was repeated while pumping a different selection of mode families, such that the scaling of the sideband strength with  $\Delta\omega_{\text{rep}}$  could be retrieved. The result shown in Fig. S.3d reveal that the mean power of the first sidebands (averaged over multiple comb lines) decreases for larger repetition rate difference, with a slope that matches a lorentzian profile with a typical linewidth of 170 kHz (full width half maximum) which is in line with the measured quality factors of the resonances.

Conversely, when measuring the optical lineshape of counter-propagating comb lines, no detectable signs of intermodulation products could be observed in any of

the  $\Delta\omega_{\text{rep}}$  configurations (Fig. S.3g). In that case, the phase matching condition cannot be fulfilled at the same time as the energy conservation unless  $\Delta\omega_{\text{rep}} = 0$ .

**Stability** In our experiments, the detuning of the laser with respect to one of the pumped modes is actively stabilised via an offset Pound-Drever-Hall (PDH) lock<sup>40</sup>. This ensures that the resonance-laser detuning remains within the soliton supporting range<sup>17</sup>, as the resonator is free-running and subject to temperature drift. With regards to the relative stability of the produced dual-comb, this means that the main source of instability is the drift of the repetition rates difference  $\Delta f_{\text{rep}}$ , since the frequency offset between the two pumps is set via electro-optic modulation. We counted the repetition rates of two counter-propagating combs and performed an Allan deviation analysis. Up to 10 ms, the repetition rates are averaging down, meaning that coherent averaging can be performed up to this duration. On longer timescales, thermal drifts dominate, but we believe that the stability can be easily improved via a thermal stabilisation scheme based on the measurement of  $\Delta f_{\text{rep}}$ .

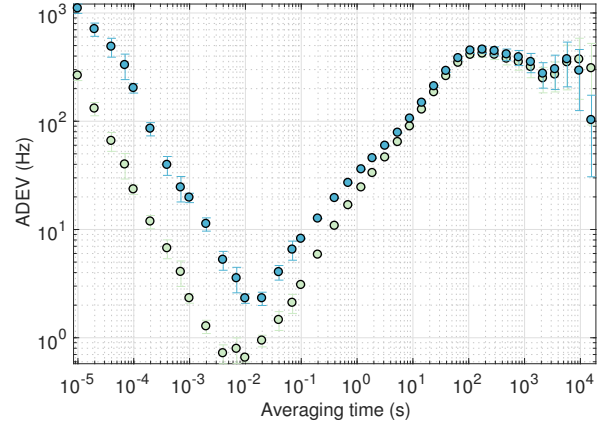


Figure S.5. Overlapping Allan deviation of the repetition rates ( $\sim 12$  GHz) of two counter-propagating combs. The marker colours corresponds to each repetition rate.